Article

Untargeted metabolomics reveals molecular effects of ketogenic diet on healthy and tumor xenograft mouse models

David Licha[1], Silvia Vidali[2], Sepideh Aminzadeh-Gohari[2], Oliver Alka[3], Leander Breitkreuz[1], Oliver Kohlbacher[3,4,5,6], Roland Reischl[1], René G. Feichtinger[2], Barbara Kofler[2]*, Christian G. Huber[1]*

[1] Bioanalytical Research Laboratories, Department of Biosciences and Cancer Cluster Salzburg, University of Salzburg, Hellbrunnerstraße 34, 5020 Salzburg, Austria; david.licha@sbg.ac.at (D.L.); leander.breitkreuz@sbg.ac.at, (L.B.); roland.reischl@sbg.ac.at (R.R.); c.huber@sbg.ac.at (C.G.H.)

[2] Research Program for Receptor Biochemistry and Tumor Metabolism, Department of Pediatrics, Paracelsus Medical University, Salzburg, 5020, Austria; s.vidali@salk.at (S.V.); s.aminzadeh-gohari@salk.at (S.A.-G.); r.feichtinger@salk.at (R.G.F.); b.kofler@salk.at (B.K.)

[3] Applied Bioinformatics, Department of Computer Science, University of Tübingen, Sand 14 72076 Tübingen, Germany; alka@informatik.uni-tuebingen.de (O.A.); oliver.kohlbacher@uni-tuebingen.de (O. K.)

[4] Institute for Bioinformatics and Medical Informatics, University of Tübingen, Sand 14, 72076 Tübingen, Germany

[5] Institute for Translational Bioinformatics, University Hospital Tübingen, Hoppe-Seyler-Str. 9, 72076 Tübingen, Germany

[6] Biomolecular Interactions, Max Planck Institute for Developmental Biology, Max-Planck-Ring 5, 72076 Tübingen, Germany

*Correspondence:

Christian G. Huber

University of Salzburg, Department of Biosciences, Bioanalytical Research Labs and Cancer Cluster Salzburg

Hellbrunnerstrasse 34, 5020 Salzburg, Austria

Tel: +43 662 8044 5738, Fax: +43 662 8044 5751, e-mail: c.huber@sbg.ac.at

Barbara Kofler

Research Program for Receptor Biochemistry and Tumor Metabolism, Department of Pediatrics

University Hospital of the Paracelsus Medical University

Müllner Hauptstraße 48, 5020, Salzburg, Austria

Tel: +43 (0)5 7255-26274, Fax: +43 (0)5 7255-58507, e-mail: b.kofler@salk.at

Abstract: Ketogenic diet (KD) is getting in the focus as auxiliary cancer therapy, since it provides sufficient energy supply for healthy cells, while impairing energy production in tumor cells underlying the Warburg effect. Thereby, it can assist in inhibiting tumor growth and simultaneously counteract cachexia, which is frequently observed in cancer patients under chemotherapy. In order to provide molecular evidence for the proposed synergistic inhibition of tumor growth, we applied untargeted quantitative metabolome analysis on a breast cancer xenograft mouse model. Healthy mice and such bearing breast cancer xenografts and receiving chemotherapy were compared after treatment with control diet and KD. Metabolomic profiling was performed on plasma samples, applying high-performance liquid chromatography coupled to tandem mass spectrometry.

44   Statistical analysis revealed metabolic fingerprints comprising numerous significantly regulated
45   features in the group of mice bearing breast cancer. This fingerprint disappeared after treatment
46   with KD, resulting in recovery to the metabolic status observed in healthy mice receiving control
47   diet. Moreover, amino acid metabolism as well as fatty acid transport were found to be affected by
48   both, the tumor and the applied KD. Our results provide clear evidence of a significant molecular
49   effect of KD in the context of tumor growth inhibition.
50
51   **Keywords:** Ketogenic diet, breast cancer, xenograft, untargeted metabolomics, HPLC-MS, reversed
52   phase chromatography, hydrophilic liquid interaction chromatography
53

1. Introduction

55   Since ketogenic diet (KD) was established in the 1920s to treat epilepsy [1], it has been under
56   investigation for many years as a potential therapy for numerous other diseases, such as Parkinson's
57   disease, Alzheimer's disease, acne, and diabetes [2-6]. In the context of tumor therapy, KD has been
58   propounded to potentiate antitumor effects of chemotherapy or radiation and to simultaneously
59   reduce needed dosages to increase the quality of life of patients [7-9]. In the long tradition of applying
60   this diet, various forms have been developed mainly differing in the fat: carbohydrate: protein ratio
61   and in the type of fat used. A traditional KD consists of a 4:1 ratio (fat: carbohydrate + protein). An
62   alternative to the traditional KD is, for example, a KD supplemented with medium-chain triglyceride
63   (MCT). Compared to long-chain triglycerides (LCT), MCTs are more rapidly absorbed into the
64   bloodstream and oxidized for energy delivery because of their ability to passively diffuse through
65   membranes. Moreover, MCTs have higher potency to increase ketone body synthesis in the liver.
66   Thus, adding MCTs to a KD might allow a less strict diet [10,11].
67   Cancer cells exhibiting the well-known "Warburg effect" are highly dependent on glucose as an
68   energy source, and show frequently low but functional oxidative phosphorylation (OXPHOS). Even
69   in the presence of oxygen, they manage their energy supply mainly *via* aerobic glycolysis, where
70   pyruvate is oxidized to lactate instead of being fueled into the citric acid cycle [12]. Targeted
71   metabolomics studies have already shown that KD leads to elevated levels of ketone bodies in
72   plasma, derived from β-oxidation of fatty acids [13]. During fasting or under a KD, acetoacetate and
73   β-hydroxybutyrate, the predominant products of ketogenesis, are supposed to replace the reduction
74   of blood glucose, as the primary source of energy. After conversion to acetyl-CoA, they are
75   introduced into the citric acid cycle, where NADH is generated to drive ATP production *via* oxidative
76   phosphorylation, which occurs in the inner mitochondrial membrane. Regarding cancer, tumor cells
77   are supposed to be strongly constricted in energy production by a combination of minimal
78   carbohydrate and extensive fat uptake, while energy supply of normal cells is assured *via* ketone
79   bodies [7,14].
80   Neuroblastoma represents a cancer type, for which the application of KD has already revealed
81   promising results in terms of inhibition of tumor growth [15,16]. In contrast, for breast cancer so far
82   there are not many preclinical studies available where KD was used [17-19]. A recent study indicated
83   that KD enhances the efficacy of targeted therapy, in particular phosphatidylinositol-3 kinase (PI3K)
84   inhibitors, and overcomes drug resistance [17]. In humans only a couple of case reports are available
85   where KD was applied in combination with other treatments [20,21]. One study showed that short
86   term KD during radiotherapy was beneficial (progression and quality of life) for a breast cancer

87　patient [22]. Since several types of breast cancer are characterized by the Warburg effect, and the KD

88　mimics a fasting diet, with the energy supply coming mostly through the catabolism of ketone bodies

89　[23], we hypothesized that application of a MCT supplemented KD as an auxiliary treatment might

90　also be beneficial in breast cancer therapy. Untargeted metabolomics (MTX) represents a powerful

91　tool to study biological processes induced by specific stimuli on the metabolome of model organisms

92　both *in vitro* and *in vivo* [24,25]. Due to its close association with the phenotype, metabolic profiling

93　might provide the most confident fundament for the correlation of observations made on the level of

94　phenotype with global changes in biomolecules and/or molecular events [26,27]. This is especially

95　important in cases, where little is known about the putative molecular effects of a certain treatment.

96　Here, untargeted analysis of the metabolome can elucidate changes of canonical pathways,

97　facilitating generation of hypotheses that can subsequently be verified *via* follow-up experiments [28].

98　　　Besides the induction of ketone body formation [7] and changes in amino acid metabolism [13],

99　global effects of KD on the metabolome are widely unknown, particularly in relation to tumor

100　growth. Therefore, we here implement xenografts of human tumors as cancer models to study the

101　effect of KD in combination with classical chemotherapy. In order to cover the broadest possible

102　range of metabolic characteristics, we examined biological effects of the therapy by untargeted HPLC-

103　MS-based metabolomic analysis, employing four different and orthogonal combinations of

104　chromatographic selectivity and mass spectrometric ionization. Using statistical data evaluation for

105　the detection of significantly regulated metabolites, we aimed at discovering biological networks and

106　pathways involved in the adaptation to KD in combination with chemotherapy. In that course,

107　further factors induced by KD that lead to impaired tumor proliferation, beside the proposed

108　induction of lowered glucose blood levels could be revealed.

109

2. Results and Discussion

2.1. Study design

In order to investigate the effects of KD on tumor growth in combination with cytostatic therapy, the plasma metabolomes of a human xenograft breast cancer model in mice was analyzed. The MTX samples were extracted from the plasma of anesthetized mice. All animals bearing tumor xenografts received cyclophosphamide (CPA) chemotherapy. Plasma of healthy *vs.* tumor bearing mice samples, which received either ketogenic or normal diets was analyzed. As a previous study revealed that a combination of long-chain triglycerides (LCT) and middle-chain triglycerides (MCT8) exerted the most potent effect on inhibition of tumor growth [16], we decided to use a LCT-MCT8 diet in the treatment experiments. Healthy mice, receiving neither chemotherapy nor KD served as negative controls (Figure 1a).

In order to maximize the number of confident metabolite identifications, we employed chromatographic separation both by reversed-phase high-performance liquid chromatography (RP-HPLC) and hydrophilic interaction liquid chromatography (HILIC) in combination with detection by electrospray ionization mass spectrometry (ESI-MS) both in positive (posESI) or negative (negESI) detection mode, as previously described [24,28]. Very stringent filtering for elimination of background signals and unstable signals utilizing custom workflows (Figure 1b) based on open-source software was performed as previously explained [24]. After detection of significantly regulated metabolite features, metabolite identification was performed on the basis of fragmentation spectra with the open-source tools Metlin, SIRIUS, and CSI:FingerID [29-33]. Finally, standard compounds were analyzed by RP-HPLC/HILIC-pos/negESI-MS/MS, yielding a database of 46 different metabolites with corresponding retention times and mass spectra (see supplementary material), which were utilized for metabolite identification at level 1 according to the criteria defined by the Metabolomics Standards Initiative [34]. Finally, biological pathway analysis using the KEGG database [35-37] was performed to reveal the metabolic effects of the different treatments.

2.2 Ketogenic diet induced effects in MDA-MB-468 tumor bearing mice

LCT-MCT8 diet (ratio of fat: carbohydrate + protein = 8:1; LCTs enriched with 25% 8-carbon MCTs; supplementary table 1) and cyclophosphamide (CPA) 30 mg/kg/day treatments significantly decreased tumor volume in MDA-MB-468 xenografts bearing mice already after the first 20 days of treatment, compared to the mice treated with CPA and control (CTRL) diet (Supplementary figure S1a). KD was well tolerated, after an initial slight weight loss, due to adaptation to the different taste and palatability of the new diets, the mice body weight stabilized and remained quite constant throughout the experiment (Supplementary figure S1b).

LCT-MCT8 diet significantly increased the concentration of blood ketone bodies in the mice already after five days of treatment (Supplementary figure S1c). In contrast, average blood glucose levels did not show any diet specific change and remained mostly unchanged until termination of the experiment after 80 days (Supplementary figure S1d).
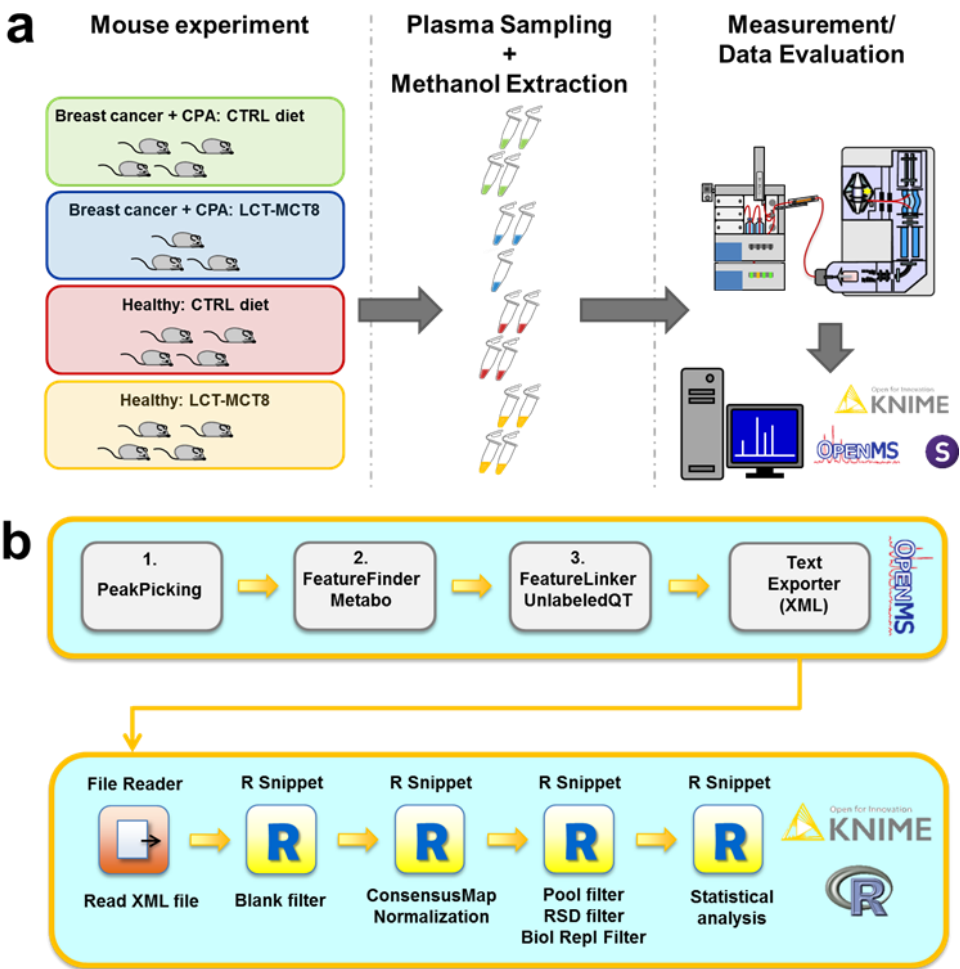
Figure 1. General (**a**) and computational workflow (**b**) applied for metabolomics studies. CPA=cyclophosphamide; LCT-MCT8=long chain triglyceride/medium-chain triglyceride diet. For details of the computational workflow, see Materials and Method section.

2.3 Results of untargeted metabolome analysis

Combining features detected in all four measurement modes and strict filtering, we obtained approximately 7,000 metabolite features in plasma of mice bearing breast cancer. This significant number of detected metabolite features represents a solid basis for further interpretation with regard to biological effects of the treatment of tumors by either chemotherapy or a combination of chemotherapy with KD. After recognition of significantly regulated features upon LIMMA (linear models for microarray data) [38] and Benjamini-Hochberg correction for multiple testing [39] (Table 1), the vast majority of detected features did not exert significant changes (corrected p-value < 0.05) in abundance comparing the different study groups. Subsequently, accurate masses of all differentially regulated metabolite features were compared with the human metabolome database (HMDB [40]) and putative molecular formulae were computed *via* SIRIUS, while the corresponding fragmentation spectra were interpreted using CSI:FingerID [29-32] and Metlin [33], which yielded 175 tentative metabolite identifications. After metabolite identification at level 1 using reference standards, a set of 34 identified and regulated metabolites was used for pathway analysis as described below.

164

165   **Table 1.** Number of significantly regulated metabolite features between differently treated mouse models.

Treatment group	Number of significantly regulated features		
	BC[a] + CPA[b] + LCT-MCT8[c]	Healthy + CTRL[d]	Healthy + LCT-MCT8
BC + CPA + CTRL	375	103	1,340
BC + CPA + LCT-MCT8	-	371	1
Healthy + CTRL	-	-	597

166   [a] Breast cancer; [b] cyclophosphamide; [c] long-chain triglycerides/medium-chain triglyceride diet; [d] control diet.
167
168
169   *2.4 Regulated metabolites upon KD treatment*

170   Comparing plasma of mice with breast cancer xenografts under chemotherapy with healthy
171   mice, both receiving a control diet showed 103 significantly regulated features (Figure 2a), either
172   induced by the tumor or the chemotherapy. This number decreased drastically when feeding a KD,
173   revealing only one significantly regulated feature (Figure 2b). The observed decrease in regulated
174   features suggests an approximation of the metabolism of mice bearing cancer to the metabolism of
175   healthy mice, under a LCT-MCT8 diet. The volcano plots in Figure 2 c and d clearly support this
176   hypothesis, whereby the left plot represents a molecular fingerprint of the tumor. Subsequently,
177   when treated with LCT-MCT8 diet, all significant down-regulations induced by the breast cancer in
178   mice fed with a control diet disappeared, leaving only one significantly upregulated feature.
179   Unfortunately, neither database search nor interpretation of fragment spectra allowed the assignment
180   of a chemical structure of this feature having an accurate mass of 282.0447 Da. Nevertheless, the lack
181   of significant regulations underlines the suppression of tumor specific effects upon LCT-MCT8 diet.
182   In this context, a heatmap (Figure 3) of the 103 significantly regulated features induced by the tumor
183   in mice fed with a control diet clearly confirms that the bulk of these regulations is reverted to the
184   levels of healthy mice fed with a control diet or even inverted, when treated with an LCT-MCT8 diet.
185   Figure 3 highlights the four identified metabolites maleic acid, 5,6-dihydrouridine, N(5)-
186   acetylornithine, and tetradecanoylcarnitine, which were downregulated in the plasma samples of
187   breast cancer bearing mice receiving the control diet but were slightly upregulated in the tumor
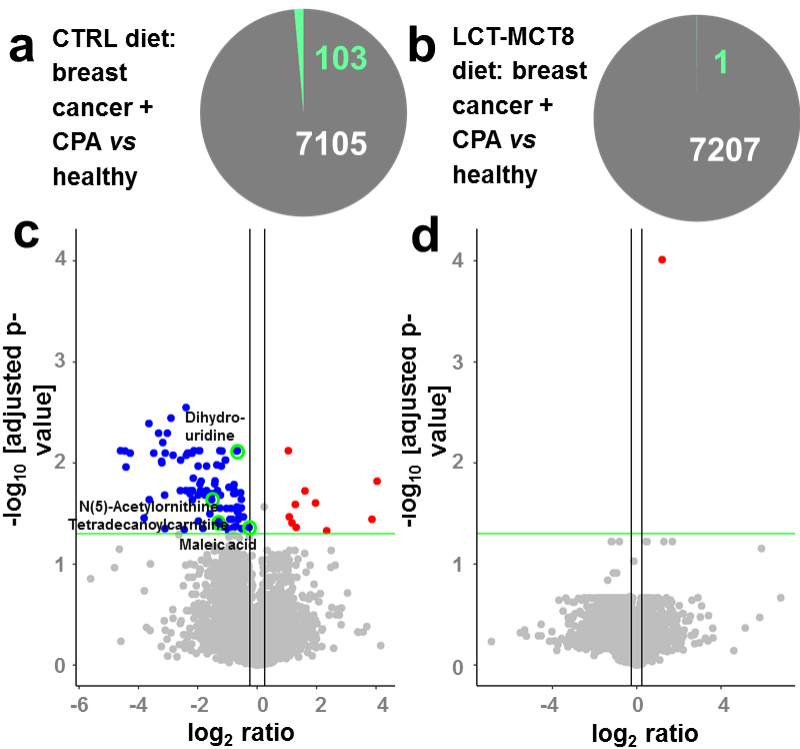188   model receiving KD (for more discussion see below).
189

Figure 2. Pie charts (**a,b**) and corresponding volcano plots (**c,d**) showing significantly regulated features induced by breast cancer under chemotherapy in mice receiving a control diet (**a,c**) and a KD (**b,d**), respectively. The volcano plots show the negative log p-value (LIMMA followed by Benjamini-Hochberg correction) against $\log_2$ ratios of regulations induced by breast cancer under chemotherapy. Blue dots represent down-regulated, red dots up-regulated and grey dots non-regulated features with a significance threshold of 0.05 (green line). Vertical black lines indicate $\log_2$ ratios of -0.25 and 0.25. Green circles indicate identified metabolites.
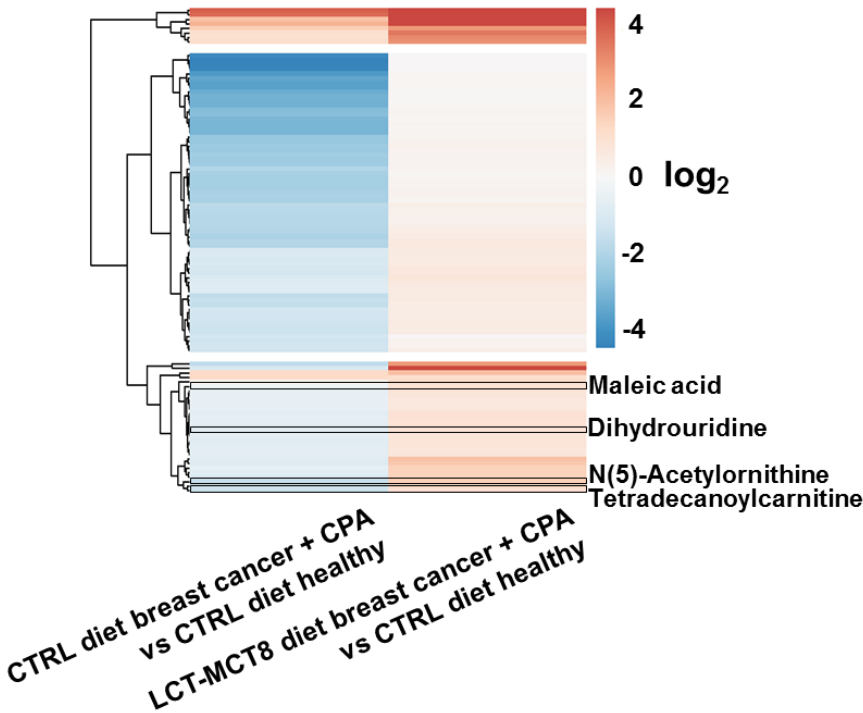

Figure 3. Heatmap of the 103 significantly regulated features induced by breast cancer under chemotherapy in mice receiving control or LCT-MCT8 diet.

201   Comparison of the mice bearing breast cancer xenografts under CPA treatment and receiving
202   LCT-MCT8 diet with the ones fed with control diet revealed 375 significantly regulated features
203   (Figure 4a, right circle of the Venn diagram). In healthy mice, the LCT-MCT8 diet induced 597
204   significant alterations (Figure 4a, left circle of the Venn diagram). The overlap between the two sets
205   of regulated metabolite features was only 16.5% (138 features), whereas the bulk of regulated features
206   differed between the two groups. This either indicates different effects of KD between healthy mice
207   and those with breast cancer or different effects of KD in combination with chemotherapy.
208   Principal Component Analysis (PCA) of all detected features from all four modes of analysis
209   (Figure 4b) unveiled distinct clustering of all four treatment groups included in the study, indicating
210   that untargeted metabolomics represents a highly useful tool to visualize changes in the metabolome
211   of biological model organisms upon certain treatments. The groups treated with KD clustered in the
212   negative sector of PC1. The cohort of mice bearing breast cancer xenografts and receiving
213   chemotherapy as well as control diet was found in the very right sector of the PCA. However, when
214   treated with an adjuvant LCT-MCT8 diet this cohort shifted horizontally in between the group of
215   healthy mice fed with a control diet and LCT-MCT8 diet, respectively. These observations reveal
216   significant differences between the metabolomes of the treatment groups, which were finally
217   confirmed by LIMMA followed by Benjamini-Hochberg correction to find regulated features to be
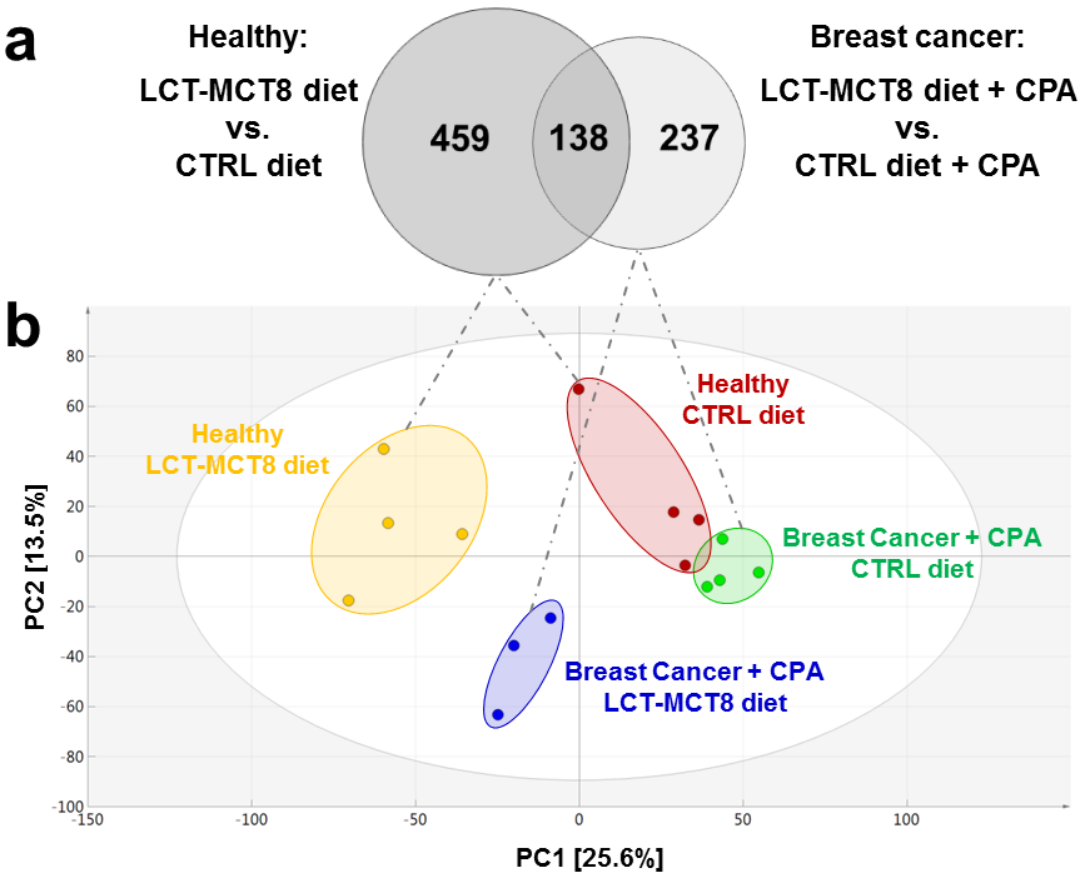218   subsequently identified *via* database searches and reference standards.
219

220
221   **Figure 4.** Overlap of significantly regulated features induced by LCT-MCT8 diet in breast cancer group *vs.*
222   healthy group (**a**) and PCA Score Scatter plots of plasma samples of breast cancer bearing mice (**b**).
223
224   *2.5 Regulations in amino acid biosynthesis and N-acetylation*

225   Several metabolites involved in the amino acid biosynthesis pathway showed a significant up-
226   regulation (LIMMA p-value after Benjamini-Hochberg correction < 0.05) upon treatment with LCT-
227   MCT8 diet. The heatmap presented in Figure 5a illustrates the regulations of nine amino acids as well
228   as five acetylated amino acids. The application of LCT-MCT8 diet generally led to an upregulation of
229   the 14 metabolites in healthy mice (column 1 in Fig. 5a). Moreover, in breast cancer bearing mice, the
230   diet led to a rather moderate increase of most levels of the nine amino acids, while upregulation of
231   N-acetylated amino acids was significantly more pronounced (column 2), which indicates a
232   prominent role of acetylation in the context of KD in tumor bearing mice (see below).
233   The metabolic context of the altered amino acids is shown in Figure 5b. Since the observed increases
234   (highlighted in red) concern a number of important nodes in the pathway, we conclude that increased
235   amino acid biosynthesis represents one of the organism's primary responses to a very limited supply
236   of protein provided by the KD (8 % in the LCT-MCT diet). However, a preclinical study on
237   neuroblastoma does not support this hypothesis. No changes in the levels of specific AAs in the
238   plasma of mice fed a control diet matching the low protein content of the KDs were observed
239   [16]. Therefore, it seems that altered AA levels in the KD group are caused by cross-talk between fat-
240   and protein-metabolic pathways.
241   Another detail revealed in the metabolite regulations is the upregulation of only three of five
242   important metabolites of the arginine biosynthesis, namely N-acetylglutamate, N(5)-acetylornithine
243   and citrulline. This suggests that high amino acid levels are not metabolized in the urea cycle, but are
244   transferred to the citric acid cycle for further energy production. N-acetylation is mediated *via* N-
245   acetyltransferases, which are important enzymes in the detoxification of medications and
246   environmental toxins [41]. Due to the elevated levels of acetylated amino acids we assume that an
247   increased expression or activation of N-acetyltransferases is induced by KD.
248
249   *2.6 Regulation of N(5)-acetylornithine and 5,6- dihydrouridine*

250   Of all the metabolites shown in the heatmap of Figure 5a, particular interest applies to N(5)-
251   acetylornithine, which was one of the four identified metabolites showing a significant regulation
252   comparing breast cancer bearing mice and healthy mice, both receiving a control diet (log_2 ratio = -
253   1.54; p-value LIMMA after Benjamini-Hochberg correction = 0.024, Figure 6a). Compared to
254   healthy/control diet, N(5)-acetylornithine is significantly down-regulated in the CPA-treated breast
255   cancer mice (Figure 6a). KD inverts this into significant up-regulation, albeit total levels remain lower
256   than in healthy, LCT-MCT8 treated mice. This implies that the down-regulation of N(5)-
257   acetylornithine was induced by the breast cancer xenograft, independent of the applied diet.
258   Moreover, the extent of up-regulation induced by the LCT-MCT8 diet is considerably higher as
259   compared to the regulation of the residual metabolites involved in amino acid biosynthesis. As can
260   be seen in Figure 6a, the decrease of N(5)-acetylornithine levels caused by the tumor is counter-
261   balanced by the LCT-MCT8 diet, so that the N(5)-acetylornithine concentration is restored to levels
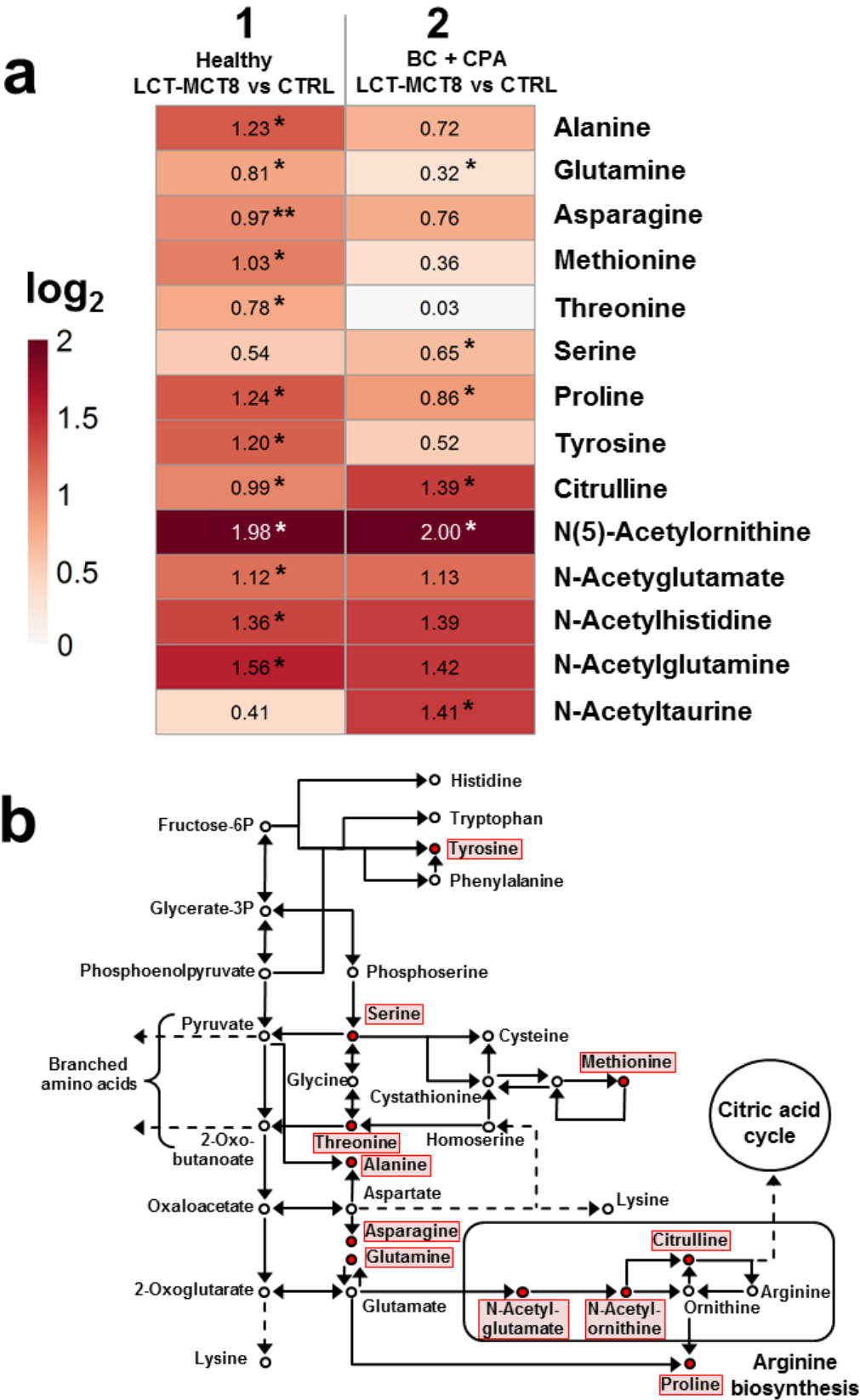262   similar to those in healthy mice fed with a control diet.
263

264
265   **Figure 5**. Heatmap of significantly regulated metabolites involved in amino acid biosynthesis induced by breast
266   cancer under chemotherapy and KD, respectively (**a**) and pathway map of amino acid biosynthesis (**b**). Red dots
267   in the pathway map [35-37] indicate metabolites showing a significant regulation induced by LCT-MCT8 diet in
268   healthy and/or in breast cancer bearing mice.

269   N(5)-acetylornithine is a minor component of deproteinized mammalian plasma and known to
270 be an intermediate in the arginine biosynthesis and in the urea cycle as a precursor of ornithine
271 (Figure 5b) [42]. Recently, increased concentrations of N(5)-acetylornithine in urine of mice have been
272 associated with aging effects. In that study, the authors suggested a correlation with a malfunction of
273 the urea cycle and subsequent diminished removal of ammonia from the body [43]. In this context,
274 Suhre *et al.* showed a connection of N-acetylated ornithine with kidney function, whereby elevated
275 concentrations were associated with lower estimated glomerular filtration rates [41]. McClay *et al.*
276 found N(5)-acetylornithine to be down-regulated by treatment of mice with haloperidol, an
277 antipsychotic drug [44]. In contrast, Napoli *et al.* observed significantly higher N(5)-acetylornithine
278 levels in human plasma of X-associated tremor/ataxia syndrome (FXTAS) patients after treatment
279 with allopregnanolone, a natural neurosteroid that induces beneficial effects in neurodegenerative
280 diseases [45]. However, none of the studies was able to provide a causal biological interpretation for
281 the observed alterations. The few published data suggest that elevated N(5)-acetylornithine
282 concentrations predominantly characterize diseased conditions. This is in contrast to our observation,
283 where cancer seems to reduce N(5)-acetylornithine levels, which can be brought back to normal levels
284 with the help of KD.

285   The 5,6-dihydrouridine concentration is significantly lower in plasma of mice bearing breast
286 cancer compared to healthy mice (Figure 6b). 5,6-Dihydrouridinylation is a posttranscriptional
287 modification of tRNA molecules, providing the required conformational flexibility to enable loop
288 formation and tertiary interactions at the same time [46]. Upon metabolomic serum analysis, elevated
289 5,6-dihydrouridine has been suggested as a potential diagnostic marker for squamous cell carcinoma
290 [47], which contrasts our results of reduced concentration. Moreover, in mice bearing breast cancer
291 xenografts and receiving a LCT-MCT8 diet, levels of 5,6-dihydrouridine were restored to the range
292 of healthy mice receiving control diet, which again corroborated the effect of KD to support
293 homeostasis. Interestingly, in healthy mice LCT-MCT8 diet also caused decreased concentrations of
294 5,6-dihydrouridine compared to the control diet.

295

296 *2.7 Fatty acid transport*

297 Carnitine is known as a key metabolite relevant for the transport of fatty acids into mitochondria,
298 where their degradation *via* ß-oxidation takes place. Thereby, the fatty acid chain is attached to
299 carnitine *via* an ester bond, resulting in an acylcarnitine [48,49]. As can be seen in Figure 6c-f, several
300 acylcarnitine derivatives were significantly regulated by KD. Along that line, stearoylcarnitine O-
301 adipoylcarnitine and 2-methylbutyrylcarnitine levels were elevated by the LCT-MCT8 diet (Figure
302 6c and d). Due to the high dietary fat uptake during a KD, increased transport and metabolism of
303 fatty acids are reasonable and in accordance with the literature [50]. Since such changes must be
304 expected in diets with high fat content, this molecule rather poses an example for the meaningfulness
305 of data generated by our metabolomics workflow.

306   On the other hand tetradecanoylcarnitine showed significant downregulation in the breast
307 cancer-bearing cohort fed with control diet (Figure 6f), revealing that the fatty acid metabolism is
308 partially dysregulated by the tumor. This trend was also observed for stearoylcarnitine, which is in
309 accordance with the publication of Wu *et al.*, who have found decreased levels of stearoylcarnitine
310 and other metabolites involved in fatty acid metabolism in a lung cancer mouse model [48]. In this

311 respect, our data suggests that the downregulation of tetradecanoylcarnitine and stearoylcarnitine
312 induced by the tumor is balanced or even reversed by KD, since both metabolites trend towards
313 increased concentrations in healthy as well as in breast cancer bearing mice when treated with a LCT-
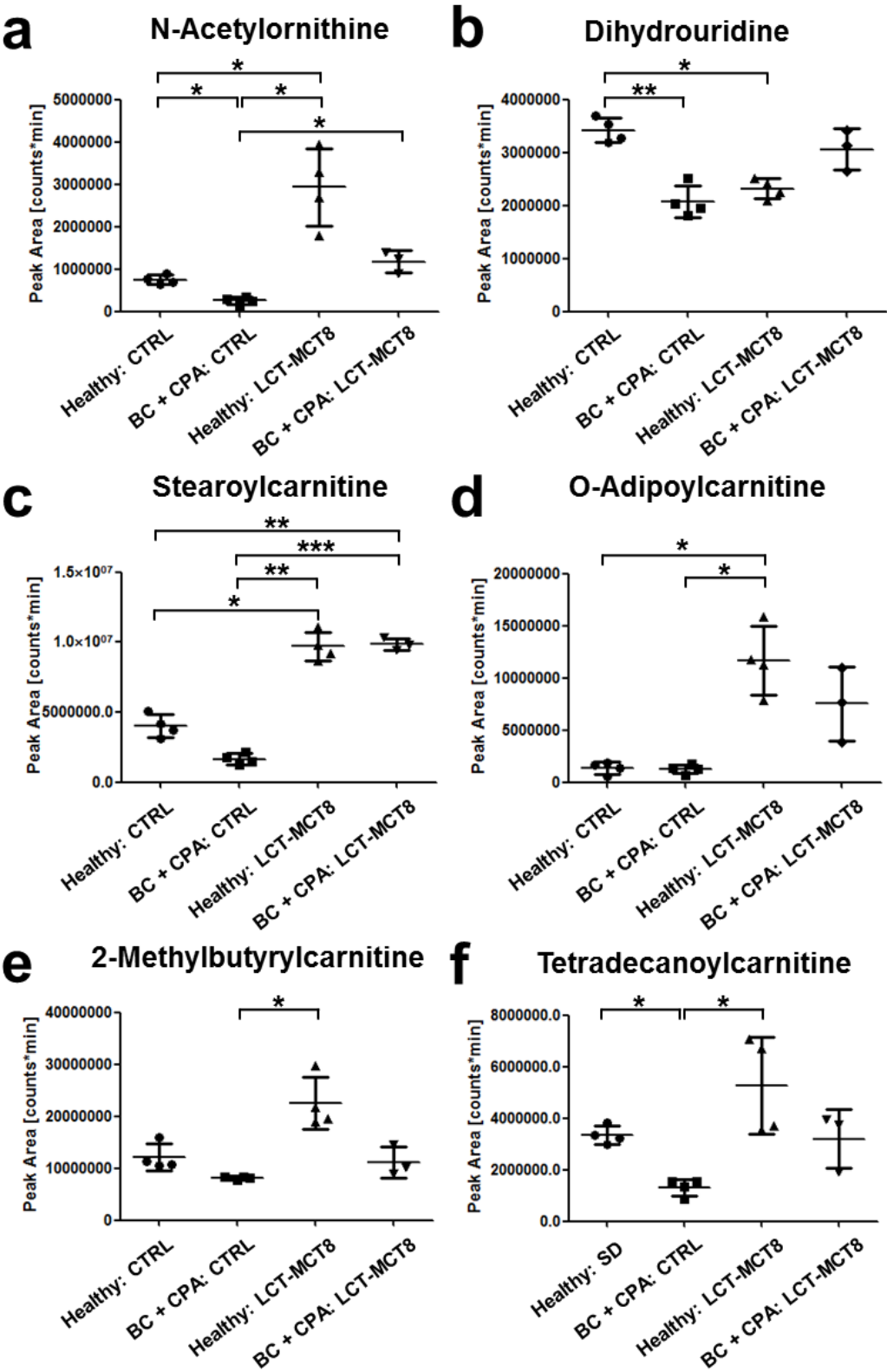314 MCT8 diet.
315

316

Figure 6. Regulation of several metabolites induced by KD and breast cancer xenografts.

317

318

319

3. Materials and Methods

3.1 Cell culture

MDA-MB-468 cell line (ATCC, HTB-132) was used for the generation of breast cancer xenografts. Cells were cultivated in high glucose DMEM medium (Sigma-Aldrich, Austria) supplemented with heat-inactivated fetal bovine serum (Gibco, Austria) and penicillin/streptomycin amphotericin B solution (Lonza, Germany).

3.2 Animal experiments

All *in vivo* experiments were performed in accordance with protocols approved for this study by the Salzburg Animal Care and Use Committee (20901-TVG/116/6-2016 for breast cancer and 20901-TVG/87/7-2014 for healthy animals). Mice were maintained under specific pathogen-free conditions and care conformed to the Austrian Act on Animal Experimentation. All experiments were performed on female CD-1 nu/nu mice (Charles River, Germany), the animals were group-housed and had unlimited access to food and water. Xenografts were established as previously described [16,51]. Briefly, a suspension of $1.5*10^7$ MDA-MB-468 cells in serum-free medium and matrigel (BD Biosciences, Austria) were injected into the right flank of 5- to 6-week-old mice.

When tumor size reached about 300 mm^3, mice were randomized into different dietary intervention groups (CTRL, LCT-MCT8; n = 5-6) [16]. The animals were group-housed and had unlimited access to food. Dietary interventions were combined with oral metronomic chemotherapy with CPA (30 mg/kg). The healthy, 7 weeks old, mice were fed with the experimental diets (CTRL, LCT-MCT8; supplementary table 1) [16,51]. All animals were monitored twice a week for body weight using a digital scale. Blood glucose and ketone body (β-hydroxybutyrate) levels were monitored once a week using a specific enzyme-based kit (Precision Xceed, Abbott Laboratories, Austria). Tumor volume was measured twice a week in the xenografts bearing mice, by using a caliper and calculating the volume according to the formula (width x height x length) / 2.

Breast cancer bearing mice were euthanized after 80 days of treatment, whereas healthy mice after 40 days. Therefore, mice were injected with 10 μl/g of anesthetic mix (ketamine 20.5 mg/ml, xylazine 5.4 mg/ml, acepromazine 270 μg/ml in saline solution), and after checking for absence of reflexes from the paw, heart puncture was performed. Mice were then immediately euthanized *via* head-neck dislocation. Blood was transferred into tubes (BD Microtainer® PSTTM LH tubes) (BD Biosciences, Austria) and plasma was collected as described in the manufacture's protocol, and snap frozen in liquid nitrogen [16,51].

3.3 Preparation of plasma samples

Metabolites were extracted by adding 810 μL of ice-cold methanol (VWR, Rednor, Pennsylvania, USA), containing 10 $\mu mol\ L^{-1}$ ethylparaben (Fluka, Buchs, Switzerland) 2 $\mu mol\ L^{-1}$ 3-nitro-L-tyrosine (Sigma-Aldrich, St. Louis, USA) and 4 $\mu mol\ L^{-1}$ d_4- succinate (Sigma-Aldrich) to 90 μL of plasma. Proteins were pelleted in a centrifuge (HERMLE, Wehingen, Germany) at 18620 rpm for 10 minutes at 4°C. The supernatant was evaporated to dryness in a vacuum concentrator (Eppendorf, Hamburg, Germany) at room temperature, followed by resuspension in 90 μL 50 % methanol.

3.4 HPLC-MS measurements

An ultra-high-performance liquid chromatography (UHPLC) system consisting of an Accela 1250 pump, a Column Oven 300 (all from Thermo Fisher Scientific, Bremen, Germany), and an LC PAL DLW Option Autosampler with a 100 mL syringe (from CTC Analytics AG, Zwingen, Switzerland) was coupled to a hybrid quadrupole-Orbitrap mass spectrometer (Model Q Exactive Plus; Thermo Fisher Scientific) equipped with a heated electrospray ion source operating in the positive or negative ion mode. A quality control sample (pool) was generated by merging an aliquot (10 μL) of all samples included in the study. Prior to injection into the HPLC-MS system, samples and pools were diluted 1:5 with Millipore water for reversed phase mode and 1:3 with acetonitrile (VWR, Rednor, Pennsylvania, USA) for HILIC mode separation.

Each sequence started with three blank runs, followed by three pool injections and finished with one pool and one blank run. In between, a blank run and a pool run were conducted after every third sample. Each sample was measured in four different selectivity and ionization mode combinations, which were RP - positive ionization, RP - negative ionization, HILIC - positive ionization and HILIC - negative ionization, resulting in four data sets per study. For each combination an exclusion list of the 100 most abundant ions obtained from prior blank runs has been generated, to avoid MS fragmentation of chemical or electronic noise signals.

For RP-HPLC separations, a 100 x 2.1mm i.d. Hypersil Gold aQ column (Thermo Fisher Scientific) packed with 1.9 μm octadecyl silica particles was applied. For column protection, a 4.0 x 3.0 mm i.d. C_{18} Security Guard pre-column (Phenomenex, Torrance, California, USA) was installed. In reversed phase mode, mobile phase A and B were Millipore water and acetonitrile, both containing 0.10 % formic acid (Sigma-Aldrich). The HPLC method started with holding 100 % A for 1.5 minutes, followed by a linear gradient to 100 % B in 6.5 minutes. After washing for 2.0 minutes at 100 % B, the column was re-equilibrated to starting conditions for 3.0 minutes, resulting in a total run time of 13.0 minutes.

HILIC-HPLC separations were performed using a 150 x 2.0 mm i.d. Nucleodur HILIC column (Macherey-Nagel, Düren, Germany), packed with 1.8 μm zwitterionic functionalized particles. Additionally, a 4.0 x 2.0 mm i.d. Nucleodur HILIC 1.8 μm pre-column, also from Macherey-Nagel was applied to protect the column. In the HILIC mode, mobile phase A contained 50 mM ammonium formate in 50 % acetonitrile, while mobile phase B was 10 mM ammonium formate (Sigma-Aldrich) in 90 % acetonitrile. After holding 100 % B for 3.0 minutes a linear gradient to 100 % A in 17.0 minutes was applied. The column was washed for 2.0 minutes at 100 % A and re-equilibrated to starting conditions for 8.0 minutes, resulting in a total run time of 30.0 minutes.

In both modes a flow rate of 0.30 μL min^{-1} and an injection volume of 2.70 μL were applied. The column temperature was held constant at 30°C. Apart from the run time of 13.0 minutes in RP mode and 30.0 minutes in HILIC mode, MS settings of the data-dependent Top 5 method were identical for both selectivity modes. Scan range and resolution of MS^1 scans were set to 80 – 850 m/z and 70000, respectively, using an AGC target of 1e6 and a maximum injection time of 50 ms. The five most abundant ions of the MS^1 scan were isolated with an isolation window of 0.8 m/z, fragmented *via* HCD applying stepped normalized collision energies of 20, 40, 60 and acquired in centroid mode. The maximum injection time was set to 64 ms with an AGC target of 5e4 at a resolution of 17500. In addition to an exclusion of charges greater than two, dynamic exclusion of 5.0 seconds was used, in

403 order to avoid multiple fragmentations of the same ions. Using these settings, all samples were
404 measured in the positive and negative ionization mode in separated sequences for each selectivity
405 and ionization mode. Tune parameters were a capillary temperature of 320°C, a probe heater
406 temperature of 350°C and an S-lens level of 50 for both ionization modes. Differing settings were a
407 sprayer voltage of 4.0 kV and 3.5 kV, sheath gas flow rate of 35 and 45, as well as an auxiliary gas
408 flow rate of 5 and 10 in positive and negative ionization mode, respectively.

409

410 *3.5 Data evaluation*

411 Acquired .raw files were converted to .mzML files using the MSConvert tool of the
412 ProteoWizard software (version 3.0.8688). Metabolomics data have been deposited to the EMBL-EBI
413 MetaboLights database [52] with the identifier MTBLS1066. The complete dataset can be accessed
414 here https://www.ebi.ac.uk/metabolights/MTBLS1066. The resulting files were further processed
415 using a bioinformatic workflow in the Konstanz Information Miner (KNIME) [53], version 3.3.4 with
416 integrated OpenMS 2.1.0 software [29] (see supplementary tables 2-6 for detailed settings). The
417 applied   KNIME   workflow   can   be   accessed   here
418 https://www.myexperiment.org/workflows/5109.html. After peak picking, feature detection and
419 feature alignment, data was filtered, normalized and statistically evaluated using Linear Models for
420 Microarray Data (LIMMA) [38] followed by Benjamini-Hochberg correction [39] for multiple testing.
421 The MTX study design and data treatment involved stringent filtering of "noise" signals or such
422 originating from the chemical background, which enabled the reduction of chemical and electronic
423 artefacts. Along that line, the HPLC-MS signals were aligned retention time wise, followed by
424 exclusion of features that did not exceed a threshold of fivefold the median intensity of the
425 corresponding signal in the blank from further data processing. In the next step, data was normalized
426 *via* a robust regression to account for variations occurring during sample preparation and
427 measurement. Features showing instable signals in the quality control runs and those not being
428 present in a sufficient number of replicates or treatment conditions were removed. Filtering was
429 based on peak area threshold in blank runs, as well as on relative standard deviation in quality control
430 samples and occurrence in biological replicates.
431 Identification was done in a multiple step approach: 1. Monoisotopic mass search in the   HMDB
432 [40]; 2. Molecular structure database search using SIRIUS in combination with CSI:FingerID [29-32];
433 3. Manual fragment spectra search against METLIN [33]; 4. Verification of database hits *via*
434 comparison of retention time and fragment spectra of reference standards. Principal Component
435 analyses were generated using SIMCA (version 13.0.3.0; Umetrics, Umea, Sweden).

436

437 *3.6 Verification of database hits with standards.*

438 All reference standards, besides N(5)-acetylornithine,   5,6 dihydrouridine and N-acetyltaurine
439 were purchased from Sigma Aldrich and measured on the same instrument using the same methods
440 as for plasma and tumor tissue samples. N(5)-acetylornithine and 5,6 dihydrouridine were customly
441 synthesized by MedChemTronica (Sollentuna, Sweden)and AKos GmbH (Lörrach, Germany)
442 respectively, while N-acetytaurine was synthesized inhouse. Retention time and MS^2 spectra
443 concordance between samples and standards was assessed manually by visual comparison.

4. Conclusions

The present study revealed molecular effects of KDs in a breast cancer mouse model. We could show that LCT-MCT8 diet can shift a derailed plasma metabolome induced by a breast cancer xenografts back to the one of healthy mice. Further, we find a strong up-regulation of amino acid metabolism as well as of amino acid N-acetylation in healthy and breast cancer bearing mice upon KD treatment. In this course, N(5)-acetylornithine, which is involved in amino acid biosynthesis as a precursor of arginine and proline is significantly down-regulated in plasma of the breast cancer xenograft group. LCT-MCT8 diet, however, induced an elevation of N(5)-acetylornithine levels back to the ones found in healthy mice fed with a control diet. This raises the interest for this metabolite and therefore requires further investigation to disclose its relevance in relation to tumor growth and treatment with KD.

Conflicts of Interest: The authors declare no conflict of interest.

Abbreviations

KD	ketogenic diet
OXPHOS	oxidative phosphorylation
MTX	metabolomics
CPA	cyclophosphamide
CTRL	control
MCT8	medium-chain triglycerides
LCT	long-chain triglycerides
RP-HPLC	reversed-phase high-performance liquid chromatography
HILIC	hydrophilic interaction liquid chromatography
ESI-MS	electrospray ionization mass spectrometry
posESI	positive electrospray ionization
negESI	negative electrospray ionization
LIMMA	linear models for microarray data
HMDB	human metabolome database
PCA	Principal Component Analysis
FXTAS	X-associated tremor/ataxia syndrome
UHPLC	ultra-high-performance liquid chromatography
KNIME	Konstanz Information Miner

466   **References**

467   1.   WILDER, R.M. In *The effects of ketonemia on the course of epilepsy*, Mayo Clin Proc, 1921;
468   pp 307-308.
469   2.   VanItallie, T.B.; Nonas, C.; Di Rocco, A.; Boyar, K.; Hyams, K.; Heymsfield, S.B.
470   Treatment of parkinson disease with diet-induced hyperketonemia: A feasibility
471   study. *Neurology* **2005**, *64*, 728-730.
472   3.   Van der Auwera, I.; Wera, S.; Van Leuven, F.; Henderson, S.T. A ketogenic diet
473   reduces amyloid beta 40 and 42 in a mouse model of alzheimer's disease. *Nutr. Metab.*
474   **2005**, *2*, 28.
475   4.   Gasior, M.; Rogawski, M.A.; Hartman, A.L. Neuroprotective and disease-modifying
476   effects of the ketogenic diet. *Behav. Pharmacol.* **2006**, *17*, 431-439.
477   5.   Paoli, A.; Grimaldi, K.; Toniolo, L.; Canato, M.; Bianco, A.; Fratter, A. Nutrition and
478   acne: Therapeutic potential of ketogenic diets. *Skin Pharmacol. and Physiol.* **2012**, *25*,
479   111-117.
480   6.   Yancy, W.S.; Foy, M.; Chalecki, A.M.; Vernon, M.C.; Westman, E.C. A low-
481   carbohydrate, ketogenic diet to treat type 2 diabetes. *Nutr. Metab.* **2005**, *2*, 34.
482   7.   Vidali, S.; Aminzadeh, S.; Lambert, B.; Rutherford, T.; Sperl, W.; Kofler, B.;
483   Feichtinger, R.G. Mitochondria: The ketogenic diet—a metabolism-based therapy.
484   *Int. J. Biochem. Cell Biol.* **2015**, *63*, 55-59.
485   8.   Allen, B.G.; Bhatia, S.K.; Buatti, J.M.; Brandt, K.E.; Lindholm, K.E.; Button, A.M.;
486   Szweda, L.I.; Smith, B.J.; Spitz, D.R.; Fath, M.A. Ketogenic diets enhance oxidative
487   stress and radio-chemo-therapy responses in lung cancer xenografts. *Clin. Cancer*
488   *Res.* **2013**.
489   9.   Klement, R.J. The emerging role of ketogenic diets in cancer treatment. *Curr Opin*
490   *Clin Nutr Metab Care* **2019**, *22*, 129-134.
491   10.   Kossoff, E.H.; Zupec-Kania, B.A.; Auvin, S.; Ballaban-Gil, K.R.; Christina Bergqvist,
492   A.; Blackford, R.; Buchhalter, J.R.; Caraballo, R.H.; Cross, J.H.; Dahlin, M.G. Optimal
493   clinical management of children receiving dietary therapies for epilepsy: Updated
494   recommendations of the international ketogenic diet study group. *Epilepsia open*
495   **2018**, *3*, 175-192.
496   11.   Page, K.A.; Williamson, A.; Yu, N.; McNay, E.C.; Dzuira, J.; McCrimmon, R.J.;
497   Sherwin, R.S. Medium-chain fatty acids improve cognitive function in intensively
498   treated type 1 diabetic patients and support in vitro synaptic transmission during
499   acute hypoglycemia. *Diabetes* **2009**, *58*, 1237-1244.
500   12.   Xu, X.D.; Shao, S.X.; Jiang, H.P.; Cao, Y.W.; Wang, Y.H.; Yang, X.C.; Wang, Y.L.;
501   Wang, X.S.; Niu, H.T. Warburg effect or reverse warburg effect? A review of cancer
502   metabolism. *Oncol Res Treat* **2015**, *38*, 117-122.
503   13.   Douris, N.; Melman, T.; Pecherer, J.M.; Pissios, P.; Flier, J.S.; Cantley, L.C.; Locasale,
504   J.W.; Maratos-Flier, E. Adaptive changes in amino acid metabolism permit normal

505   longevity in mice consuming a low-carbohydrate ketogenic diet. *Biochim. Biophys.*
506   *Acta, Mol. Basis Dis.* **2015**, *1852*, 2056-2065.

507   14.   Zhou, W.; Mukherjee, P.; Kiebish, M.A.; Markis, W.T.; Mantis, J.G.; Seyfried, T.N.
508   The calorically restricted ketogenic diet, an effective alternative therapy for
509   malignant brain cancer. *Nutr. Metab.* **2007**, *4*, 5.

510   15.   Morscher, R.J.; Aminzadeh-Gohari, S.; Feichtinger, R.G.; Mayr, J.A.; Lang, R.;
511   Neureiter, D.; Sperl, W.; Kofler, B. Inhibition of neuroblastoma tumor growth by
512   ketogenic diet and/or calorie restriction in a cd1-nu mouse model. *PloS one* **2015**, *10*,
513   e0129802.

514   16.   Aminzadeh-Gohari, S.; Feichtinger, R.G.; Vidali, S.; Locker, F.; Rutherford, T.;
515   O'Donnel, M.; Stöger-Kleiber, A.; Mayr, J.A.; Sperl, W.; Kofler, B. A ketogenic diet
516   supplemented with medium-chain triglycerides enhances the anti-tumor and anti-
517   angiogenic efficacy of chemotherapy on neuroblastoma xenografts in a cd1-nu
518   mouse model. *Oncotarget* **2017**, *8*, 64728-64744.

519   17.   Hopkins, B.D.; Pauli, C.; Du, X.; Wang, D.G.; Li, X.; Wu, D.; Amadiume, S.C.;
520   Goncalves, M.D.; Hodakoski, C.; Lundquist, M.R. Suppression of insulin feedback
521   enhances the efficacy of pi3k inhibitors. *Nature* **2018**, *560*, 499.

522   18.   Zhuang, Y.; Chan, D.K.; Haugrud, A.B.; Miskimins, W.K. Mechanisms by which low
523   glucose enhances the cytotoxicity of metformin to cancer cells both in vitro and in
524   vivo. *PloS one* **2014**, *9*, e108444.

525   19.   Gluschnaider, U.; Hertz, R.; Ohayon, S.; Smeir, E.; Smets, M.; Pikarsky, E.; Bar-Tana,
526   J. Long-chain fatty acid analogues suppress breast tumorigenesis and progression.
527   *Cancer Res.* **2014**, *74*, 6991-7002.

528   20.   İyikesici, M.S.; Slocum, A.K.; Slocum, A.; Berkarda, F.B.; Kalamian, M.; Seyfried, T.N.
529   Efficacy of metabolically supported chemotherapy combined with ketogenic diet,
530   hyperthermia, and hyperbaric oxygen therapy for stage iv triple-negative breast
531   cancer. *Cureus* **2017**, *9*.

532   21.   Branca, J.J.; Pacini, S.; Ruggiero, M. Effects of pre-surgical vitamin d
533   supplementation and ketogenic diet in a patient with recurrent breast cancer.
534   *Anticancer Res.* **2015**, *35*, 5525-5532.

535   22.   Klement, R.J.; Sweeney, R.A. Impact of a ketogenic diet intervention during
536   radiotherapy on body composition: I. Initial clinical experience with six
537   prospectively studied patients. *BMC Res. Notes* **2016**, *9*, 143.

538   23.   Balasse, E.O.; Féry, F. Ketone body production and disposal: Effects of fasting,
539   diabetes, and exercise. *Diabetes Metab Rev.* **1989**, *5*, 247-270.

540   24.   Ranninger, C.; Rurik, M.; Limonciel, A.; Ruzek, S.; Reischl, R.; Wilmes, A.; Jennings,
541   P.; Hewitt, P.; Dekant, W.; Kohlbacher, O. Nephron toxicity profiling via untargeted
542   metabolome analysis employing a high performance liquid chromatography-mass
543   spectrometry-based experimental and computational pipeline. *J. Biol. Chem.* **2015**,
544   *290*, 19121-19132.

545   25.   Rattigan, K.M.; Pountain, A.W.; Regnault, C.; Achcar, F.; Vincent, I.M.; Goodyear,
546   C.S.; Barrett, M.P. Metabolomic profiling of macrophages determines the discrete

547   metabolomic signature and metabolomic interactome triggered by polarising
548   immune stimuli. *PloS one* **2018**, *13*, e0194126.

549 26. León, Z.; García-Cañaveras, J.C.; Donato, M.T.; Lahoz, A. Mammalian cell
550   metabolomics: Experimental design and sample preparation. *ELECTROPHORESIS*
551   **2013**, *34*, 2762-2775.

552 27. Homuth, G.; Teumer, A.; Völker, U.; Nauck, M. A description of large-scale
553   metabolomics studies: Increasing value by combining metabolomics with genome-
554   wide snp genotyping and transcriptional profiling. *J. Endocrinol.* **2012**, *215*, 17-28.

555 28. Boyles, M.S.P.; Ranninger, C.; Reischl, R.; Rurik, M.; Tessadri, R.; Kohlbacher, O.;
556   Duschl, A.; Huber, C.G. Copper oxide nanoparticle toxicity profiling using
557   untargeted metabolomics. *Part. Fibre Toxicol.* **2016**, *13*, 49.

558 29. Röst, H.L.; Sachsenberg, T.; Aiche, S.; Bielow, C.; Weisser, H.; Aicheler, F.; Andreotti,
559   S.; Ehrlich, H.-C.; Gutenbrunner, P.; Kenar, E., *et al.* Openms: A flexible open-source
560   software platform for mass spectrometry data analysis. *Nat. Methods* **2016**, *13*, 741.

561 30. Böcker, S.; Letzel, M.C.; Lipták, Z.; Pervukhin, A. Sirius: Decomposing isotope
562   patterns for metabolite identification. *Bioinformatics* **2008**, *25*, 218-224.

563 31. Böcker, S.; Dührkop, K. Fragmentation trees reloaded. *Journal of cheminformatics* **2016**,
564   *8*, 5.

565 32. Dührkop, K.; Shen, H.; Meusel, M.; Rousu, J.; Böcker, S. Searching molecular
566   structure databases with tandem mass spectra using csi: Fingerid. *Proc. Natl. Acad.*
567   *Sci. U.S.A.* **2015**, *112*, 12580-12585.

568 33. Smith, C.A.; O'Maille, G.; Want, E.J.; Qin, C.; Trauger, S.A.; Brandon, T.R.; Custodio,
569   D.E.; Abagyan, R.; Siuzdak, G. Metlin: A metabolite mass spectral database. *Ther.*
570   *Drug Monitoring* **2005**, *27*, 747-751.

571 34. Sumner, L.W.; Amberg, A.; Barrett, D.; Beale, M.H.; Beger, R.; Daykin, C.A.; Fan,
572   T.W.-M.; Fiehn, O.; Goodacre, R.; Griffin, J.L. Proposed minimum reporting
573   standards for chemical analysis. *Metabolomics* **2007**, *3*, 211-221.

574 35. Kanehisa, M.; Goto, S. Kegg: Kyoto encyclopedia of genes and genomes. *Nucleic*
575   *Acids Res.* **2000**, *28*, 27-30.

576 36. Morishima, K.; Tanabe, M.; Furumichi, M.; Kanehisa, M.; Sato, Y. Kegg: New
577   perspectives on genomes, pathways, diseases and drugs. *Nucleic Acids Res.* **2016**, *45*,
578   D353-D361.

579 37. Morishima, K.; Tanabe, M.; Furumichi, M.; Kanehisa, M.; Sato, Y. New approach for
580   understanding genome variations in kegg. *Nucleic Acids Res.* **2018**, *47*, D590-D595.

581 38. Smyth, G.K. Linear models and empirical bayes methods for assessing differential
582   expression in microarray experiments. *Stat. Appl. Genet. Mol. Biol.* **2004**, *3*, 1-25.

583 39. Hochberg, Y.; Benjamini, Y. More powerful procedures for multiple significance
584   testing. *Stat. Med.* **1990**, *9*, 811-818.

585 40. Wishart, D.S.; Jewison, T.; Guo, A.C.; Wilson, M.; Knox, C.; Liu, Y.; Djoumbou, Y.;
586   Mandal, R.; Aziat, F.; Dong, E. Hmdb 3.0—the human metabolome database in 2013.
587   *Nucleic Acids Res.* **2012**, *41*, D801-D807.

588   41.   Suhre, K.; Shin, S.-Y.; Petersen, A.-K.; Mohney, R.P.; Meredith, D.; Wägele, B.;
589   Altmaier, E.; CardioGram; Deloukas, P.; Erdmann, J., *et al.* Human metabolic
590   individuality in biomedical and pharmaceutical research. *Nature* **2011**, *477*, 54.

591   42.   Armstrong, M.D. N-delta-acetylornithine and s-methylcysteine in blood plasma.
592   *Biochim Biophys Acta* **1979**, *587*, 638-642.

593   43.   Sun, J.; Jiao, C.; Ma, Y.; Chen, J.; Wu, W.; Liu, S. Anti-ageing effect of red ginseng
594   revealed by urinary metabonomics using rrlc-q-tof-ms. *Phytochem Anal* **2018**, *29*, 387-
595   397.

596   44.   McClay, J.L.; Vunck, S.A.; Batman, A.M.; Crowley, J.J.; Vann, R.E.; Beardsley, P.M.;
597   van den Oord, E.J. Neurochemical metabolomics reveals disruption to sphingolipid
598   metabolism following chronic haloperidol administration. *J. Neuroimmune
599   Pharmacol.* **2015**, *10*, 425-434.

600   45.   Napoli, E.; Schneider, A.; Wang, J.Y.; Trivedi, A.; Carrillo, N.R.; Tassone, F.;
601   Rogawski, M.; Hagerman, R.J.; Giulivi, C. Allopregnanolone treatment improves
602   plasma metabolomic profile associated with gaba metabolism in fragile x-associated
603   tremor/ataxia syndrome: A pilot study. *Mol. Neurobiol.* **2018**.

604   46.   Dalluge, J.J.; Hashizume, T.; Sopchik, A.E.; McCloskey, J.A.; Davis, D.R.
605   Conformational flexibility in rna: The role of dihydrouridine. *Nucleic Acids Res.* **1996**,
606   *24*, 1073-1079.

607   47.   Sridharan, G.; Ramani, P.; Patankar, S. Serum metabolomics in oral leukoplakia and
608   oral squamous cell carcinoma. *J. Cancer Res. Ther.* **2017**, *13*, 556.

609   48.   Wu, H.; Chen, Y.; Li, Z.; Liu, X. Untargeted metabolomics profiles delineate
610   metabolic alterations in mouse plasma during lung carcinoma development using
611   uplc-qtof/ms in mse mode. *Royal Soc. Open Sci.* **2018**, *5*, 181143.

612   49.   Wilcken, B. Disorders of the carnitine cycle and detection by newborn screening. *Ann
613   Acad Med Singapore* **2008**, *37*, 71-73.

614   50.   Berry-Kravis, E.; Booth, G.; Sanchez, A.C.; Woodbury-Kolb, J. Carnitine levels and
615   the ketogenic diet. *Epilepsia* **2001**, *42*, 1445-1451.

616   51.   Vidali, S.; Aminzadeh-Gohari, S.; Feichtinger, R.G.; Vatrinet, R.; Koller, A.; Locker,
617   F.; Rutherford, T.; O'Donnell, M.; Stöger-Kleiber, A.; Lambert, B., *et al.* The ketogenic
618   diet is not feasible as a therapy in a cd-1 nu/nu mouse model of renal cell carcinoma
619   with features of stauffer's syndrome. *Oncotarget* **2017**, *8*, 57201-57215.

620   52.   Haug, K.; Salek, R.M.; Conesa, P.; Hastings, J.; de Matos, P.; Rijnbeek, M.;
621   Mahendraker, T.; Williams, M.; Neumann, S.; Rocca-Serra, P. Metabolights—an
622   open-access general-purpose repository for metabolomics studies and associated
623   meta-data. *Nucleic Acids Res.* **2012**, *41*, D781-D786.

624   53.   Berthold, M.R.; Cebron, N.; Dill, F.; Gabriel, T.R.; Kötter, T.; Meinl, T.; Ohl, P.; Thiel,
625   K.; Wiswedel, B. Knime-the konstanz information miner: Version 2.0 and beyond.
626   *AcM SIGKDD explorations Newsletter* **2009**, *11*, 26-31.

627